European Polymer Journal 46 (2010) 1975–1987

Contents lists available at ScienceDirect

European Polymer Journal

journal homepage: www.elsevier.com/locate/europolj

Macromolecular Nanotechnology

Hydrogen bonding and mechanical properties of thin films of polyether-based polyurethane–silica nanocomposites

Lahorija Bistričić [a,*], Goran Baranović [b], Mirela Leskovac [c], Emi Govorčin Bajsić [c]

[a] Department of Applied Physics, Faculty of Electrical Engineering and Computing, University of Zagreb, Unska 3, 10000 Zagreb, Croatia
[b] Rudjer Bošković Institute, P.O. Box 1016, 10001 Zagreb, Croatia
[c] Faculty of Chemical Engineering and Technology, University of Zagreb, Marulićev trg 19, 10000 Zagreb, Croatia

ARTICLE INFO

Article history:
Received 26 March 2010
Received in revised form 28 July 2010
Accepted 5 August 2010
Available online 17 August 2010

Keywords:
Polyurethane
Thin films
Nanocomposites
Silica
Hydrogen bond

ABSTRACT

Two series of thin films of polyether-based polyurethane–silica nanocomposites having hard segment content of 51% and 34% and different concentrations of SiO_2 nanoparticles (0, 0.5, 1.0 and 3.0 vol.%) have been prepared. Infrared linear dichroic (LDIR) ratio, mechanical and differential scanning calorimetry (DSC) measurements were performed in order to determine the influence of hydrogen bonding on their mechanical and thermal properties. The degree of phase separation (DPS) and orientational functions in dependence on strain were calculated from the polarized IR spectra. The presence of silica nanoparticles gives rise to significant differences in the mechanical (stress–strain) properties of the nanocomposites with regard to the pure polymer. The nanocomposite thin films with lower hard segment content (HSC) displayed decreased stiffness and tensile and increased elongation at break in comparison to the nanocomposites with higher HSC. There was no distinctive influence of nanoparticles on the glass transition temperatures of soft segments. Nanosilica significantly affected the melting behavior of the hard phase only in samples with higher HSC.

1. Introduction

In the field of nanotechnology polymer nanocomposites have been attracting large interest with regard to the possibility of producing novel materials with high potential for new applications. The incorporation of nanoscale inorganic species (like, for example, TiO_2, SiO_2, ZnO and $CaCO_3$) in organic polymers can change their physical properties (thermal, mechanical, dielectric and magnetic) [1–4]. Nanosilica has been used as inorganic filler in polymers because of its high surface area and stability. It can be used for reinforcement of polymer matrices to lower shrinkage on curing, decrease thermal expansion coefficients and improve adhesion properties and corrosion resistance [5–7].

Polyurethanes (PU) are unique polymeric materials with wide range of chemical and physical properties. These materials meet highly diversified demands of modern applications being used as shape memory polymers, adhesives, foams, fiber, thermoplastic elastomers and coatings [8–10]. The specific structural features of PU and in particular PU elastomers is their two-phase microstructure which arises from the thermodynamic incompatibility between hard urethane segments and soft polyester or polyether segments. The morphology of PU consists of a continuous soft segment matrix and hard segment domains and depends also on chemical structure of PU chains, polarity of their structural fragments, sizes and molecular weight of hard and soft segments [11]. The micro-phase separation affects the physical and mechanical properties of PU, e.g. its hardness and modulus of elasticity, abrasion resistance and scratch resistance [8]. It is determined, *inter alia*, by competitive hydrogen bonding between different segments and the crystallizability of hard

* Corresponding author. Tel.: +385 1 6129 622; fax: +385 385 1 6129 605.
E-mail address: lahorija.bistricic@fer.hr (L. Bistričić).

0014-3057/$ - see front matter © 2010 Elsevier Ltd. All rights reserved.
doi:10.1016/j.eurpolymj.2010.08.001

and soft segments, methods of polymerization during synthesis, the nature of interfacial regions between the soft segment matrix and hard segment domains etc. The extent of the micro-phase separation is essential if a thermoplastic elastomer with good mechanical properties is to be made. Such a correlation of the molecular structure of a ETPU polymer and interactions with nanosilica with their macroscopic properties is essential in designing nanocomposites with desired properties for specific technical applications.

In recent years, nanocomposites of polyester-based PU with nanosilica have been studied extensively [12–17]. The addition of nanosilica improved thermal, rheological and mechanical and adhesion properties of polyester-based PU due to the formation of hydrogen bonds between the silanol groups on the nanosilica surface and the ester carbonyl groups in soft segments [15–17]. In that type of nanocomposites nanosilica enhances the incompatibility between hard and soft segments favoring the phase separation [12,13]. The addition of nanosilica increase the polyester chain mobility allowing this segment to become more ordered in relation to the pure polymer [15]. It has been shown that the introduction of the nanosilica up to 3 wt.% can significantly enhanced both tensile and elongation at break of polymer films.

Analogous studies of polyether-based PU (ETPU) thin films and their silica nanocomposites are seemingly lot less abundant. ETPUs without nanofiller are neither particularly good nor particularly poor when machanical properties such as tensile or abrasion resistance are considered [18]. Hydophilic pyrogenic nanosilica is often used for reinforcement of certain types of silicone rubbers. In this study we are going to see if similar reinforcement can be achieved in thermoplastic urethanes because hydrogen bonding is likely to be formed at the ETPU-filler interface causing a reinforcement effect. To the best of our knowledge, there is only one report on polyether-based PU silica nanocomposites [19]. The main objective in this work was thus to examine the influence of an inorganic filler on mechanical and thermal properties and thus indirectly on micro-phase separation by studying the intensity changes in the IR spectra by means of linear dichroism method. In polyester PU, nanosilica primarly interacts with carbonyl groups in soft segments [15–17]. As reported in our previous investigation also on polyester PU, it was difficult to perform spectroscopic investigation on the participation of carbonyl groups in hydrogen bonding due to the presence of C=O groups in hard as well as in soft segments [4]. In this research there is no such dificulty since the polyether-based PU have C=O groups only in hard segments and a shape of the C=O stretching band can be less ambigously partitioned into different contributions.

Two polyether-based polyurethanes (ETPU-1, ETPU-2) with different hard segment contents (51% and 34%, respectively) have been synthesized (Elastomeric TPUs contain 60–70% by weight of soft segments [11] and consequently only ETPU-2 is elastomeric). Two series of ETPU-1 and ETPU-2 silica nanocomposite thin films were also prepared with addition of different volume fractions of silica nanoparticles (0, 0.5, 1.0 and 3 vol.%). Special attention was paid to the analysis of hydrogen bonding between nanosilica and polymer chains. We used LDIR (infrared linear dichroism) to understand the influence of nanosilica on the degree of micro-phase separation through the study of the orientation of hard and soft segments as a function of applied mechanical force.

2. Experimental

2.1. Synthesis of polyurethane prepolymers

The PU prepolymers were prepared at 80° under nitrogen atmosphere in a stirred-glass reaction kettle. The diphenyl methane-4,4′-diisocyanate (MDI) was first charged into the kettle and heated up to 80°. Then an appropriate amount of polyether-based poly(tetramethylene)glycol (PTMEG, $HO–(–(CH_2)_4–O–)_{n\approx14}–H$) of 1000 molecular weight was added. The NCO/OH ratios of 4/1 (ETPU-1) and 2/1 (ETPU-2) were employed [20]. The reaction was considered completed when the experimental and calculated values of the NCO concentration were within one percent. The NCO content of isocyanates and prepolymers was measured by the di-(*n*-butyl) amine titration method.

2.2. Preparation of polyurethane elastomers

A chain extender 1,4-butanediol (BD) was added to the prepolymer with intensive mixing at the temperature of 90°. After 60 s of mixing, the reaction mixture was immediately poured into a preheated Teflon-coated aluminium mold. The mixture was then heated to 100° in a Carver hydraulic platen press for about 30 min. The polyether-based elastomers were postcured in an oven for 24 h at 105° immediately after molding [20]. The hard segment content (HSC) of the prepared elastomers was 51% for ETPU-1 and 34% for ETPU-2. The former can thus be viewed as a hard and the latter as a soft rubber [21]. The chemical structure of ETPU is shown in Fig. 1.

2.3. Preparation of polyurethane nanocomposites

Aerosil®200, a type of hydrophilic pyrogenic nanosilica (nano-SiO_2), with primary particle size of 12 nm and specific area of 200 m^2/g provided by Degussa was used as a filler in the polyurethane composites. Aerosil®200 is fumed silica appearing in the form of a fluffy powder having tamped density of only 50 kg/m^3.

Synthesized polyurethane films were dissolved in dimethylformamide without and with addition of 0.5, 1 and 3 vol.% of nano-SiO_2 and homogenized with magnetic stirrer (500 rpm). The solution was cast onto the glass plate to a uniform thickness using hand coater (designed to provide a certain film thickness). The samples were dried at the room temperature to the constant weight. In this way covalent bonding between silica nanoparticles and the polyurethane molecules has been avoided and the hydrogen bonding was expected to play the major role at the interfaces. The final thickness of prepared films was approximately 30 μm.

Lee et al. [19] also prepared their samples via *in situ* polymerization but with nanosilica added already during preparation of prepolymer. Therefore one might expect

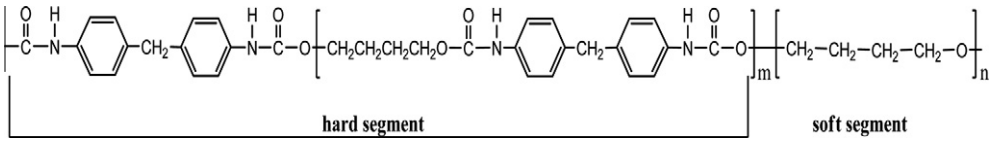

Fig. 1. Chemical structure of ETPU.

different extent of silica aggregation in this and our set of nanocomposites. They used PTMEG and Aerosil®R972 (diameter 16 nm and specific area 110 m^2/g). The synthesized nanocomposites contained 0, 1, 3, 5, 7 and 10 wt.% nanosilica. On the other hand, starting from the same raw materials except that instead of silica montmorillonite was used, the same procedure as here was applied to obtain montmorillonite/polyurethane nanocomposites [22].

2.4. Infrared measurements

For IR measurements the ETPU films were cut in strips of dimension $(20 \times 10)\,mm^2$. The stretching of samples was performed manually by a home-made extensor in 5 mm steps starting from the initial length $L_0 = 20$ mm. The IR dichroic measurements were performed on the strips that were cut in longitudinal direction to the film axis preparation.

The FTIR absorbance spectra of neat ETPU and ETPU-silica nanocomposite thin films were recorded using a Bomem MB 102 spectrometer. The extensor containing the stretched sample was placed in the spectrometer arid zone. A ZnSe IR polarizer placed in front of the sample was used to produce an incident beam of parallel and perpendicular polarization to the stretching direction. The two kind of spectra, A_p (parallel polarization) and A_n (perpendicular polarization), were collected with a resolution of $4\,cm^{-1}$ by co-adding the results of 10 scans. The spectra were always collected from a sample that was first stretched and then kept at a given length for 20 min to allow for relaxation in the stretched state. A reference spectrum was collected before each measurement.

2.5. Mechanical measurements

Mechanical measurements were performed on a Zwick Universal testing machine (model 1445) in uniaxial tension mode at 23° and 65% of relative humidity. Tensile tests were performed at constant strain rate of 10 mm/min and 40 mm gauge length. The results are shown as stress vs. strain curves. Tensile hysteresis was examined by stretching the sample in a cyclic way with a maximum deformation of 50% and 100% using cross head speed of $10\,mm\,min^{-1}$. Permanent set was reported as the percent strain at which stress dropped to zero on the reverse cycle in the hysteresis test.

2.6. Differential scanning calorimetry

The DSC measurement was made using a Mettler Toledo DSC 823^e with Intracooler. The mass of the specimens was about 10 mg. All measurements were performed in nitrogen atmosphere ($50\,cm^3$/min), and heating rate 10°/min. The specimens were cooled from 25° to −90°, held at this temperature for 10 min and subsequently heated to 250°.

3. Results and discussion

3.1. FTIR analysis

3.1.1. Poisson's ratio

Generally, in the case of small deformations it is assumed that $\frac{\Delta l}{l} = \frac{\Delta e}{e} = -\sigma\frac{\Delta L}{L}$, where σ is Poisson's ratio, L is the length of the sample, l is the width and e is the thickness. When deformations are not small as in the case of stretched polymer ribbon, a more precise formula can be used, for example, $\frac{e_s}{e_i} = 1 - \nu \ln\frac{L_s}{L_i}$ or $\frac{\Delta e}{e} = -\nu \ln\left(1 + \frac{\Delta L}{L}\right)$ what gives $\frac{A_s}{A_i} = 1 - \nu \ln\alpha$ and Poisson's ratio is obtained from the slope. A_s and A_i are the average absorbances of the extended and unstrained sample, respectively (average absorbance is $\frac{1}{3}(A_p + 2A_n)$). The absorbances A_s/A_i versus $\ln\alpha$ of the 1732 and 1703 cm^{-1} bands for the ETPU-1 and ETPU-2 samples are shown in Figs. 2 and 3. Only the plots for ETPU2, ETPU2 + 0.5% SiO_2 and ETPU2 + 1.0% SiO_2 samples are approximately linear vs. $\ln\alpha$ at strains below 300%). The corresponding values for Poisson's ratios for the 1703 cm^{-1} band are: 0.41 ± 0.01, 0.36 ± 0.05 and 0.36 ± 0.01, respectively. The ETPU2 nanocomposites have smaller values for Poisson's ratios in comparison to the pristine sample. The two bands observed at 1732 and 1703 cm^{-1} show only roughly the same behavior within the experimental error. The probable cause might be the dependence of the absorption coefficient on the deformation.

3.1.2. Degree of phase separation (DPS)

The FTIR spectra of the ETPU-1 and ETPU-2 films are presented in Fig. 4. They are very similar except in some regions that will be specified below. The positions of the bands characteristic of the functional groups remain the same in all the samples. No additional vibrational bands at 1073 and 811 cm^{-1} due to silica were observed because of its low concentrations. However, there are significant differences concerning the band intensities in the NH (3500–3200 cm^{-1}), C=O (1800–1600 cm^{-1}) as well as in the C–O–C stretching (1200–1000 cm^{-1}) regions (Figs. 4–7). The former two regions are characteristics of hard segments (Fig. 1).

The urethane and ether groups take part in the formation of hydrogen bonds. In a pure ETPU three types of hydrogen bonds can be formed between NH groups and proton accepting oxygen in (i) urethane C=O groups, (ii) urethane alkoxy groups and (iii) ether C–O–C groups. The

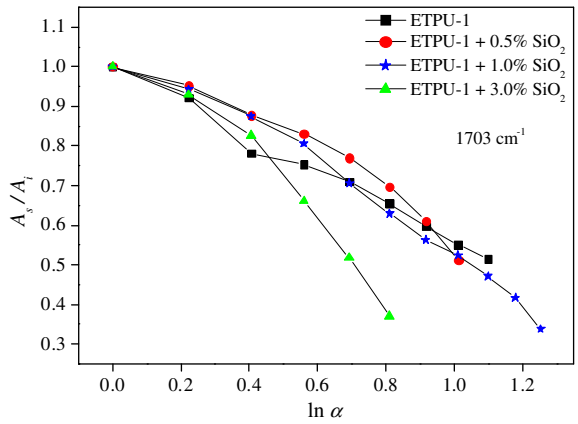

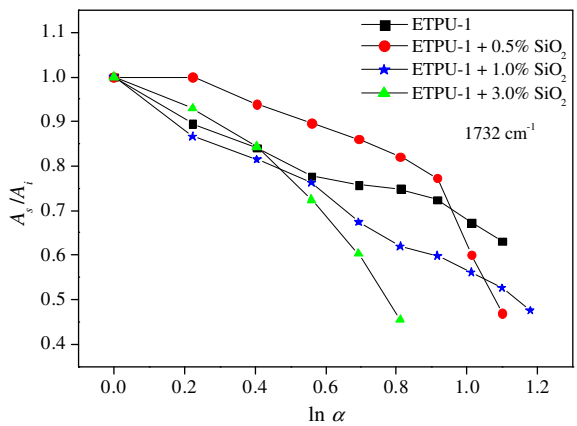

Fig. 2. The dependence of the absorbance A_s/A_i of C=O stretching bands at 1703 and 1732 cm^{-1} for ETPU-1 nanocomposites.

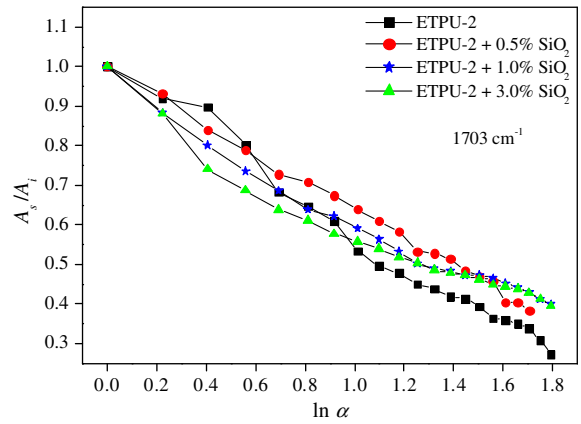

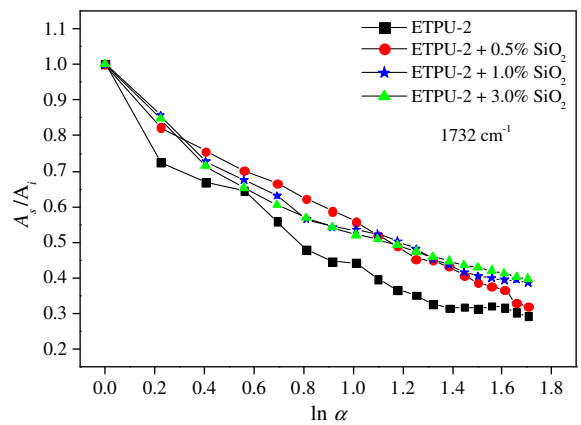

Fig. 3. The dependence of the absorbance A_s/A_i of C=O stretching bands at 1703 and 1732 cm^{-1} for ETPU-2 nanocomposites.

type and the strength of the hydrogen bonds are usually recognized by the magnitude of the wavenumber shifts. Traditionally, the N–H···O=C hydrogen bond between two urethane group has been considered the strongest. However, recent studies have shown that N–H···O (ether) bond is slightly stronger than N–H···O=C urethane bond [23–25]. On the other hand, it is known that the primary hydrogen bond acceptor depends on the length the soft segments and the concentration of the hard segments in a chain [26].

A competition between urethane and ether oxygen atoms in forming hydrogen bonds with NH is reflected in the N–H stretching region (Fig. 5). A broad band between 3400 and 3200 cm^{-1} is observed. The curve fitting of those asymmetric bands has been performed with two or three Gaussian curves. The most intensive band observed at 3330 cm^{-1} is assigned to the N–H stretching vibrations in hydrogen bond to carbonyl group (hard–hard segment interactions). The additional band at 3275 cm^{-1} corresponds to the N–H stretching vibrations hydrogen bonded to ether oxygen (hard–soft segment interactions) [27]. In the spectra of ETPU films in the N–H stretching region there was no evidence of hydrogen bonding between N–H and urethane C–O–C groups (alkoxy oxygen), i.e. no shoulder or clearly separated band is seen between 3300 and 3275 cm^{-1} where it is expected to be found according to calculations.

FTIR spectra in the carbonyl stretching region are presented in Fig 6. All the spectra were resolved into two spectral components, the one at 1703 cm^{-1} assigned to the hydrogen bonding between hard segments and also between silanol groups of nanosilica and urethane carbonyl groups. The other at 1732 cm^{-1} corresponds to the stretching vibration of free carbonyl group of hard segments.

The changes observed in the 1200–950 cm^{-1} region are connected to different interactions in which C–O–C groups participate (Fig. 7). The band observed at 1114 cm^{-1} was attributed to the antisymmetric stretching vibrations of the non-associated ether C–O–C group because it was also observed in IR spectra of pure PTMEG [25]. Urethane groups (alkoxy oxygens) display a characteristic C–O–C stretching at 1082 cm^{-1} [25]. The band observed as a shoulder at 1070 cm^{-1} in ETPU-1 and at 1077 cm^{-1} in ETPU-2 could be attributed to the hydrogen bonding interaction between N–H and C–O–C groups, i.e. to the associated ether C–O–C groups. The analyzed vibrational bands and their assignment are presented in Table 1.

The micro-phase separation can be characterized by the degree of phase separation (DPS) for a film of a given thickness that is generally evaluated by the following relation:

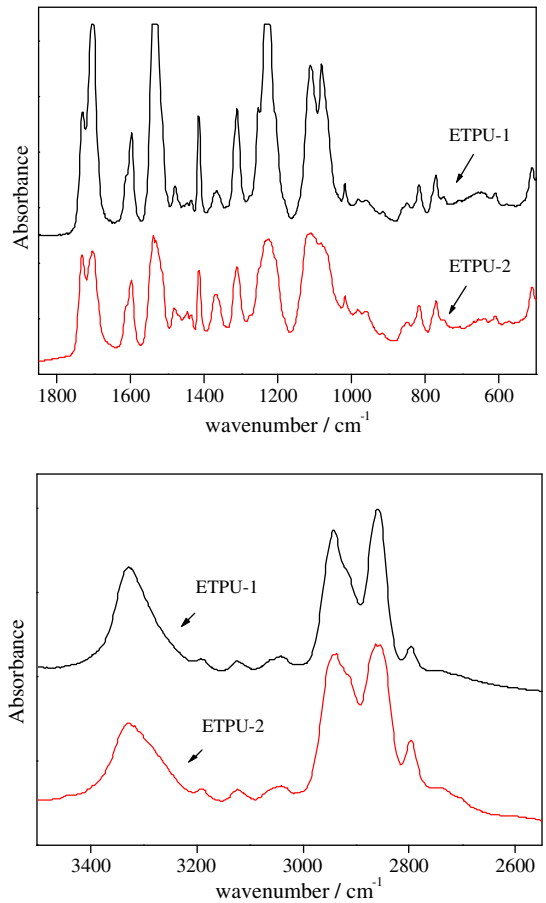

Fig. 4. Absorbance spectra of the unstretched neat ETPU-1 and ETPU-2 thin films.

$$\mathrm{DPS} = \frac{A_b}{A_b + A_f} = \frac{N_b \varepsilon_b}{N_b \varepsilon_b + N_f \varepsilon_f}$$

where A_b and A_f are the integrated absorbances (ε_b and ε_f are extinction coefficients) of hydrogen bonded and free molecular group, respectively. In other words, the limiting values of DPS, i.e. 0 and 1, refer to the single phase systems. DPS is approximately equal to $N_b/(N_b + N_f) \equiv N_{\mathrm{total}}$ provided $\varepsilon_b \approx \varepsilon_f$.

The NH groups can form hydrogen bonds with ether oxygen atoms, O_E, from the soft segments, N–H···O_E, with carbonyl oxygens, N–H···O_C, and with urethane alkoxy oxygens, N–H···O_A. The corresponding absorbances are A_E, A_C and A_A, respectively and the DPS from the N–H stretching absorptions is

$$\mathrm{DPS_{NH}} = \frac{A_{\mathrm{NH},b}}{A_{\mathrm{NH},b} + A_{\mathrm{NH},f}} \equiv \frac{A_C + A_E + A_A}{A_C + A_E + A_A + A_{\mathrm{NH},f}} \equiv \mathrm{DPS_{NH,C}} + \mathrm{DPS_{NH,E}} + \mathrm{DPS_{NH,A}}.$$

The DPS based on the carbonyl absorption is

$$\mathrm{DPS_{CO}} = \frac{A_{\mathrm{CO},b}}{A_{\mathrm{CO},b} + A_{\mathrm{CO},f}} \equiv DPS_{\mathrm{CO,N}} + DPS_{\mathrm{CO,S}} \equiv \frac{N_{\mathrm{CO,N}}\varepsilon_{\mathrm{CO,N}} + N_{\mathrm{CO,S}}\varepsilon_{\mathrm{CO,S}}}{N_{\mathrm{CO,N}}\varepsilon_{\mathrm{CO,N}} + N_{\mathrm{CO,S}}\varepsilon_{\mathrm{CO,S}} + N_{\mathrm{CO},f}\varepsilon_{\mathrm{CO},f}},$$

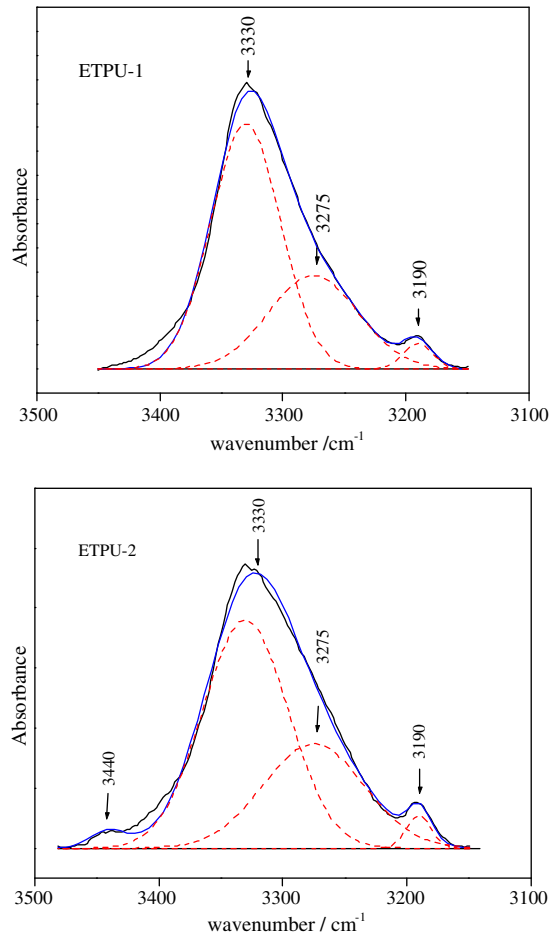

Fig. 5. Absorbance spectra of neat ETPU films in the N–H stretching region. The band at 3190 $\mathrm{cm^{-1}}$ is due to the CH aromatic stretching vibrations.

where $A_{\mathrm{CO},b}$ contains contributions of the N–H···O═C and SiO–H···O═C hydrogen bonds, A_N and A_S, respectively ($A_{\mathrm{CO},b} = A_N + A_S$). The equality $\varepsilon_{\mathrm{CO,N}} \approx \varepsilon_{\mathrm{CO,S}} \approx \varepsilon_{\mathrm{CO},f}$ is hardly acceptable although the value of $\varepsilon_{\mathrm{CO,N}}/\varepsilon_{\mathrm{CO},f}$ is probably between 1.0 and 1.2 [26].

The ν(NH) and ν(C═O) bands were deconvoluted using Gaussian shape and the obtained values of DPS for ETPU thin films, as well as for their silica nanocomposites are given in Table 2. The fraction of hydrogen bonded carbonyls equal to $\mathrm{DPS_{CO,N}}$ is a measure of phase separation, i.e. it tells something about the occurrence and the size of hard segments if it were not for the SiO–H···O═C hydrogen bonds that could not be observed. Since $\mathrm{DPS_{CO,S}}$ can be considered small, $\mathrm{DPS_{CO,N}}$ will be approximated by $\mathrm{DPS_{CO}}$. Obviously, $\mathrm{DPS_{CO,N}}$ and $\mathrm{DPS_{NH,C}}$ should be equal and they actually are within the experimental error (Table 2). About 35–40% of the NH groups are associated with ether oxygen linkage.

It is known that in pure ETPU hydrogen bonded components are expected only in hard domains, while the free ones can exist only dispersed in soft domains. The analysis has revealed that all of the NH groups in ETPU-1 were

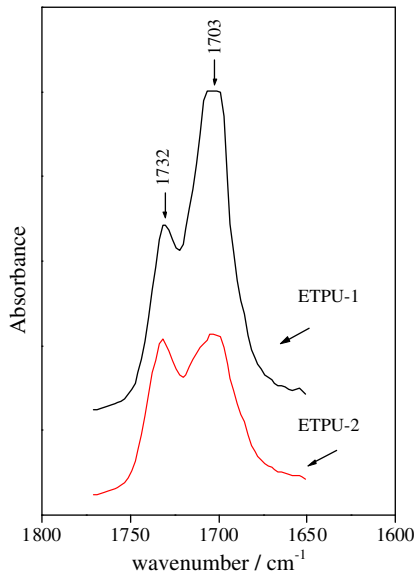

Fig. 6. The absorbance spectra in the C=O stretching region (hard segments) of neat films.

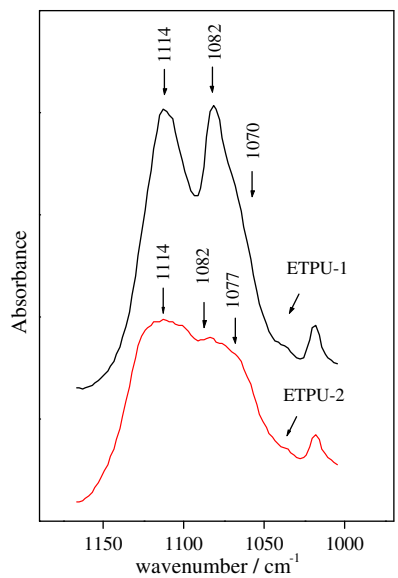

Fig. 7. The absorbance spectra in the C–O–C stretching region (soft and hard segments) of neat films.

hydrogen bonded, while only 2% of them were free in ETPU-2 (Fig. 5). The comparison of $DPS_{NH,C}$ of neat ETPU films shows that in ETPU-1 slightly more NH bonds are engaged in the hydrogen bonding within hard segments. In the neat ETPU-2 film 62% of the N–H oscillators were hydrogen bonded in hard domains. Obviously the microphase separation is more prominent in ETPU-1 than in ETPU-2. The addition of nanosilica does not significantly affect the number of hydrogen bonded NH groups. About 30% of the ETPU-1 NH groups are hydrogen bonded to the ether oxygens. No significant changes in DPS_{NH} of the nanocomposites with straining have been observed.

Table 1
The selection of observed IR frequencies (cm^{-1}) for ETPU-1 and ETPU-2[a].

ETPU-1	ETPU-2	Assignment
	3440	N–H stretching (nonbonded)
3330	3330	N–H stretching (bonded to C=O)
3275	3275	N–H stretching (bonded to C–O–C)
3190	3190	CH aromatic stretching vibrations
1732	1732	C=O stretching (nonbonded)
1703	1703	C=O stretching (bonded)
1114	1114	Antisymmetric C–O stretching of ether C–O–C (nonbonded)
1082	1082	C–O stretching of urethane C–O–C (nonbonded)
1070	1077	Antisymmetric C–O stretching of ether C–O–C (bonded)

[a] The addition of SiO_2 does not change the position of vibrational bands in ETPU-1 and ETPU-2 nanocomposites. Assignment according to Refs. [23–27].

The number of hydrogen bonded carbonyl groups is practically not affected by adding nanosilica, although the hydrogen bond interactions between the silanol groups and the C=O groups not involved in hydrogen bonding within the hard domains seem very likely. The band due to the SiO–H···O=C hydrogen bonds is present, but due to their small number no extra structure of the 1703 cm^{-1} band could be observed. This means that A_{1703} contains also other contributions, not only from the hydrogen bonding within hard domains. Again, no significant changes in DPS_{CO} of the nanocomposites with straining have been observed. According to these results, very small number of hydrogen bonds breaks during stretching deformation for ε up to 400%. Unlike the nanocomposites with montmorillonite [22], the ones filled with silica show no DPS dependence on the amount of added silica. Thus, stretching appears to have no effect on the hydrogen bonding network even for the nanocomposites or the restoration of the disrupted hydrogen bonds is so fast that it cannot be monitored by the techniques here applied. This implies other reason for the mechanical hysteresis than the disruption of the hydrogen bonding network [26].

The analysis of the vibrational bands connected to C–O stretching vibrations in ether C–O–C groups shows that in the ETPU-1 sample there are about 33–35% hydrogen bonded C–O–C groups. The addition of nanosilica has no influence on the number of bonded C–O–C groups or this effect is so small that could not be quantified. This confirms our findings that in ETPU-1 nanocomposites nanosilica interact with hard segments.

Unfortunately, in pure ETPU-2 nanocomposites the analysis of C–O stretching bands in ether C–O–C group was not possible because of their high intensities. These bands were observed within acceptable range only in the highly stretched films. Due to the very significant band overlapping at 1077 and 1082 cm^{-1} we have estimated the number of nonbonded ether C–O–C groups in highly stretched films. In neat ETPU-2 about 55% C–O–C ether groups was nonbonded. The addition of 0.5% SiO_2 decreased the number of nonbonded C–O–C ether groups to 52% due to the hydrogen bonding between soft segments and nanosilica. Further increase in SiO_2 content (1% and 3%) increased the number of nonbonded C–O–C ether

Table 2
DPS calculated from the C=O and N–H stretching bands.

ε[a] (%)	DPS_{CO}[b]					DPS_{NH}[c]				
	0	50	125	250	400	0	50	125	250	400
ETPU-1 HSC = 51%	0.69	0.70	0.67	–	–	0.68	0.68	0.69	–	–
ETPU-1 + 0.5% SiO_2	0.79	0.79	0.72	–	–	0.70	0.69	0.69	–	–
ETPU-1 + 1.0% SiO_2	0.80	0.78	0.74	–	–	0.70	0.70	0.69	–	–
ETPU-1 + 3.0% SiO_2	0.77	0.77	0.73	–	–	0.69	0.69	0.68	–	–
ETPU-2 HSC = 34%	0.61	0.67	0.67	0.67	0.64	0.62	0.62	0.62	0.62	0.61
ETPU-2 + 0.5% SiO_2	0.63	0.66	0.66	0.66	0.63	0.64	0.64	0.65	0.66	0.62
ETPU-2 + 1.0% SiO_2	0.64	0.65	0.65	0.64	0.63	0.65	0.63	0.63	0.65	0.64
ETPU-2 + 3.0% SiO_2	0.64	0.66	0.66	0.66	0.66	0.63	0.63	0.64	0.62	0.64

[a] ε, strain.
[b] $A_{1703}/(A_{1732} + A_{1703})$.
[c] $A_{3330}/(A_{3440} + A_{3330} + A_{3275})$, what should be equal to $A_{1703}/(A_{1732} + A_{1703})$, but it is not because the latter also contains the contribution from SiO-H···O = C hydrogen bonds that are not directly observable as an extra band, but are certainly present.

groups to 62% probably due to the aggregation of nanoparticles. Due to the very low intensity of band at 3440 cm^{-1} there was no evidence of increased number of free NH groups.

3.2. Orientation functions of ETPU segments

The dichroic ratio R is defined as:

$$R = \frac{A_p}{A_n}$$

where A_p and A_n are integrated absorbances of the investigated band measured with the light polarized parallel and perpendicular to the stretching direction, respectively. They are evaluated by integrating the respective absorption bands after the baseline corrections. The Gaussian functions were fitted to the experimental bands and the half-widths and intensities were allowed to vary during iteration. The maximum error associated with the fit was estimated to be less than 5%. Thus, this technique can be used to determine the orientation of specific chemical groups in multiphase systems.

The alignment of the hard and soft chain segments can be quantified using Herman orientation function [28,29]. The orientation function is related to a dichroic ratio R of an absorption band and defined as:

$$f = \langle P_2(\cos\theta)\rangle = \frac{1}{2}\left(3\langle\cos^2\theta\rangle - 1\right) = \frac{R_0 + 2}{R_0 - 1}\cdot\frac{R - 1}{R + 2} \qquad (1)$$

Where $R_0 = 2 \cdot ctg^2\beta$, β is the angle between the transition moment and the local chain axis (in the gas phase approximation here applied it is assumed that the absorption from the whole polymer is just the linear sum of the absorptions of independent molecular groups) and θ is the angle between stretching direction and the local chain axis of the polymer or any directional vector characteristic of a given chain segment. The value of the orientation function f can be shown to vary from $-1/2$ for perpendicular alignment ($\langle\cos^2\theta\rangle = 0$), to zero for random chain orientation ($\langle\cos^2\theta\rangle = 1/3$ for random values of θ in spherical polar co-ordinates), and then to unity for perfect chain alignment along the draw axis ($\langle\cos^2\theta\rangle = 1$).

The orientation function graphs were generated using Eq. (1). A transition moment direction to the chain axis (β) of 90° was assumed for the N–H stretching band, while the transition moment for carbonyl stretching was assumed to be at an angle of 79° to the chain axis [30]. When studying the alignment of the soft segments it was assumed that the transition moment of the C–O–C mode lies exactly along the molecular axis of soft segments, i.e. β was taken to be 0. Upon deformation all the groups orient themselves into the stretching direction, i.e. there are no negative values of the orientation function. However, the orientation behavior of the two types of segments should be quite different. Soft segment orientation is little affected by polymer composition and it is into the stretching direction. Hard segment orientation is strongly influenced by polymer composition. Polyurethanes possessing crystalline domains show perpendicular orientation.

The 1703 cm^{-1} band is representative of the orientation of hard chain segments in the hard domains while the band observed at 1732 cm^{-1} represents hard segments in the intermediate phase [8]. The orientation of the hard segments that are hydrogen bonded in hard domains as a function of the applied strain is presented in Fig. 8, while the orientation of hard segments in the intermediate phase is shown in Fig. 9. That the orientation functions for the 1732 and 1703 cm^{-1} vibrations are different simply is a consequence of different surroundings of free and hydrogen bonded C=O oscillators. The latter are within the hard domains and the sensitivity of the corresponding orientation function on stretching might be interpreted as an indication of the increase of hard domain order (hard domains can hardly be changed by mechanical deformations, i.e. they behave as units during straining). The hard segments are randomly oriented at 0% strain and it remains so in the ETPU-1 samples up to 25% strain. For ε below 200% the alignment of hard segments in pure ETPU-1 was greater (f = 0.18) than in pure ETPU-2 (f = 0.08) (Fig. 8). The hydrogen bonds are equally strong in ETPU-1 and -2, although their numbers are different.

It has been also found in this work that the orientation in the strain direction is highly dependent on the silica concentration. The addition of SiO_2 reduced the alignment of hard segments in ETPU-1 silica nanocomposite films. In ETPU-1 + 3% SiO_2 it was not even possible to orient hard domains. There is an appreciable difference in orientation of hard segments in ETPU-2 nanocomposites. The addition

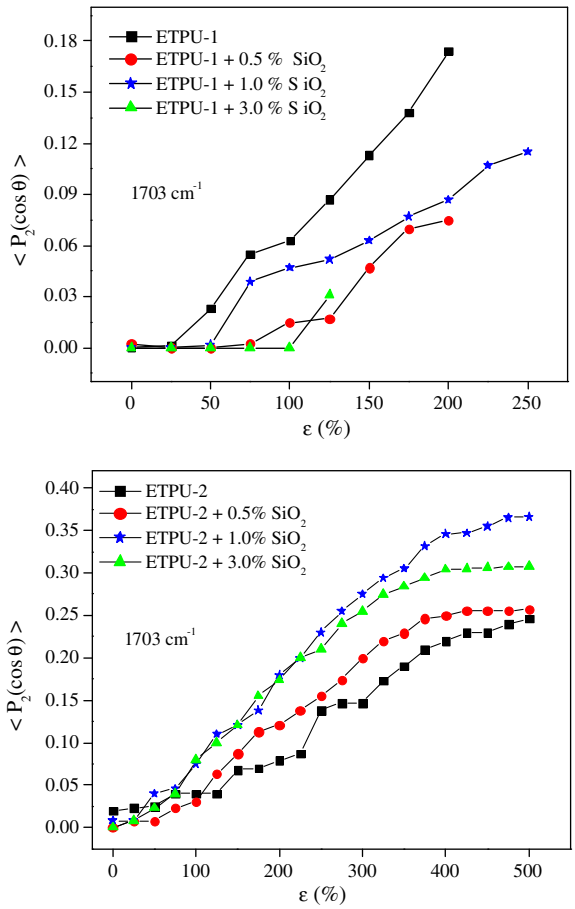

Fig. 8. The variations of the orientation function of hard segments based on the carbonyl stretching band at 1703 cm^{-1} upon stretching (the greatest ε_b values from Table 3 are smaller than those shown here because in IR measurements a film was drawn to the breakage, i.e. long after the microholes have occurred).

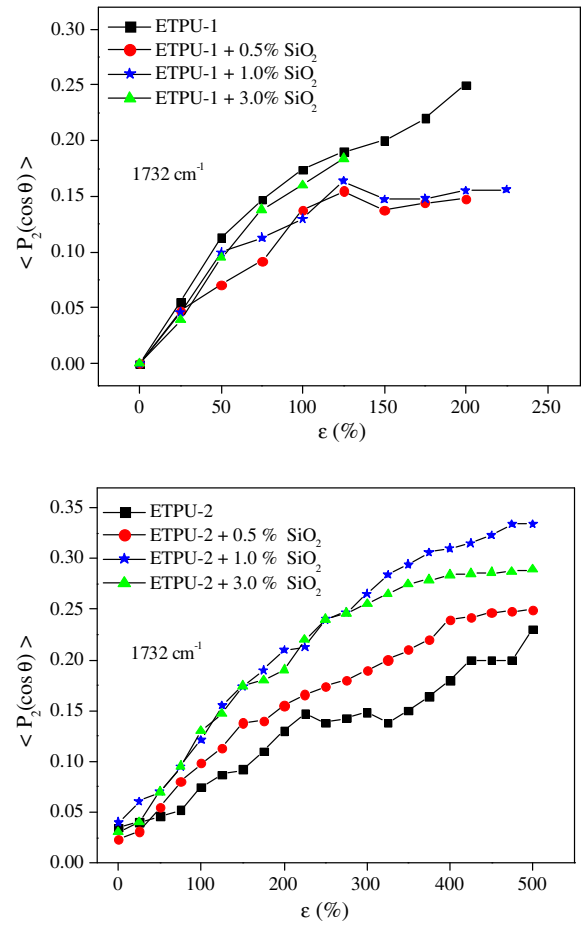

Fig. 9. The orientation of hard segments dispersed in mixed phase as a function of applied strain.

of the filler leads to the greater orientation of hard segments. The samples with 1% and 3% SiO_2 show almost identical orientation behavior for 0–250% strain. This decrease in orientation in the former case and increase in the latter is obviously associated with polymer–filler interaction. The hydrogen bonding between nanosilica and urethane C=O groups leads to immobilization of hard segments whose mobility is reduced or enhanced with regard to that of the soft polymer matrix depending on the HSC. It would be important to know whether silica remained in the form of uniformly distributed particles or were they present in the form of larger agglomerates. The latter is very likely because they are sticky and may prefer to stay close to each other (according to Merabia et al. an average size of aggregates is 100 nm [31]), particularly due to the fact that the filler was added and homogenized by stirring in already synthesized PU.

The C–O–C (ether) stretching vibrations are indicative of the orientation of the soft segments and could be thus analyzed using the bands observed at 1114 and around 1070 cm^{-1}. Unfortunately, in some samples these bands were observed within an acceptable range only in the highly stretched films (Figs. 10 and 11). The C–O–C stretching mode observed at 1114 cm^{-1} was used to characterize the orientation of the free soft segments while the band at 1070 cm^{-1} was taken to be due to the associated C–O–C groups (Fig. 10). The alignment of soft segments along the stretching direction in pure ETPU-1 was slightly smaller than the alignment of free hard segments. The results showed that the presence of nanoparticles in ETPU-1 reduced alignment of soft segments. The orientation function calculated from the absorbance of the C–O–C stretching band at 1070 cm^{-1} in ETPU-1 showed similar behavior as the band at 1732 cm^{-1}. In pure ETPU-2 the alignment of soft segments in the stretching direction as estimated from the 1114 cm^{-1} band was almost negligible due to the increased content of soft segments in comparison to pure ETPU-1 sample (Fig. 10). The analysis of orientational behavior of the soft segments in ETPU-2 nanocomposites has shown the increase in the alignment of soft segments due to the presence of nanoparticles. The alignment was dependent on the nanofiller concentration and was particularly pronounced in the ETPU-2 + 1% SiO_2 film. The orientation function calculated from 1077 cm^{-1} band in ETPU-2

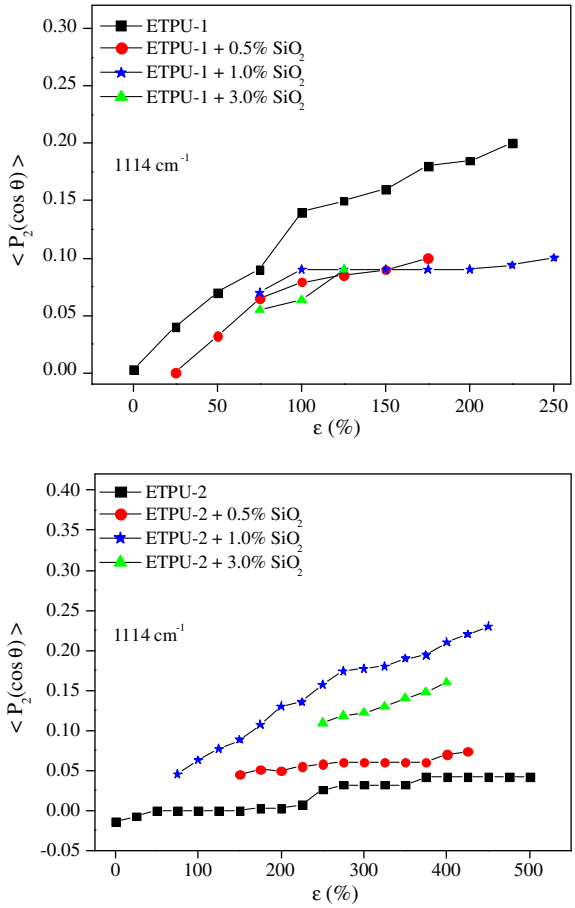

Fig. 10. Soft segments orientation as a function of applied strain (from the C–O–C band).

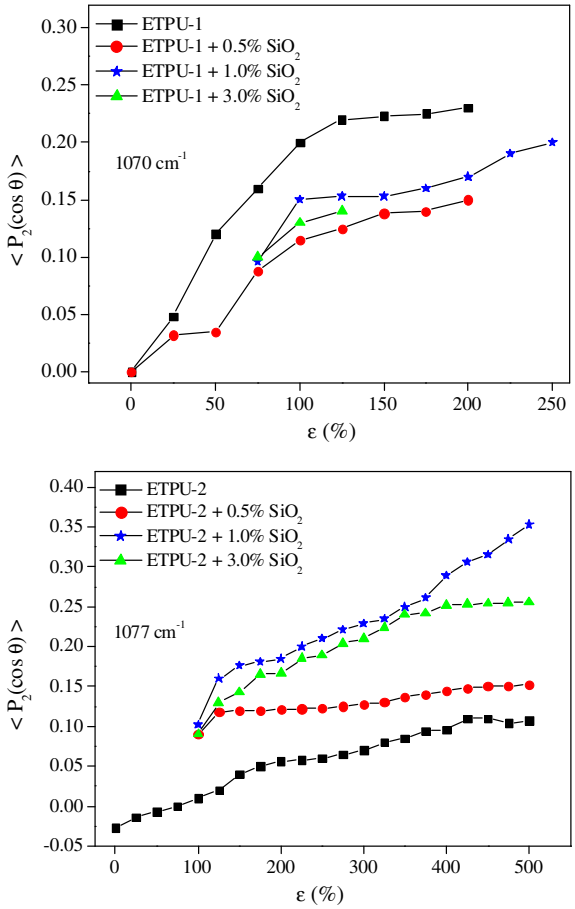

Fig. 11. Hard and soft segments orientation as a function of applied strain (from the C–O–C band).

nanocomposites displayed complex behavior during stretching. The orientation function in ETPU-2 + 0.5% SiO_2 sample display analogous behavior that was observed for soft segments, but the values of orientation function were slightly greater due to the hydrogen bonding between silanol group at the silica surface and C–O–C (ether) groups. The degree of alignment in ETPU-2 + 1.0% SiO_2 and ETPU-2 + 3.0% SiO_2 films in the stretching direction increased continuously during the orientation process. It should be noted that this orientation behavior was very similar to the behavior of hard segments in intermediate phase. This observation confirmed our assignment of the analyzed band.

3.3. Mechanical properties

As for any other polymer mechanical properties of ETPU nanocomposites are closely related to their composition and morphology. The results of mechanical testing (stress–strain curve (Fig. 12 and Table 3) and strain–hysteresis data (Fig. 13 and in Tables 4 and 5) showed expected behavior of the morphology vs. relative amount of hard and soft domains, their ordering and interaction with nanofiller. The shape of the stress–strain curve of the ETPU-2 samples with lower HSC (Fig. 12) is typical for elastomeric materials with hard domains dispersed in matrix of soft segments [21]. Since the SSC was nearly 50%, in the ETPU-1 and 70% in ETPU-2 samples the former can be considered as a hard rubber unlike the latter which would belong to soft rubbers (only with SSC being around 70% the material is soft thermoplastic rubber [21]). With decreasing hard segment content (HSC = 34%) in ETPU-2, Young modulus (E_2) decreased significantly $\left(\frac{E_1}{E_2} \approx 7\right)$, but the elongation at break and work to break were about five times greater (Table 3). As expected, the elastomeric properties of ETPU were enhanced with the increase in the SSC.

By adding nanosilica into the ETPU-1 matrix, the stiffness and strenght are decreased and the elongation at break increased, as a consequence of the changed microphase separation although it is impossible to describe the changes more thoroughly. The value of stretching stress at break was the smallest for ETPU-1 nanocomposites with 1 vol.% nanofiller. The addition of nano-SiO_2 in ETPU-1 the elongation at break was increased. The ETPU-2 nanocomposites showed slightly different behavior. The addition of 1 and 3 vol.% nanosilica into the ETPU-2 matrix progressively increases Young modulus (Table 3) and strenght with slightly changed elongation at break. Although the

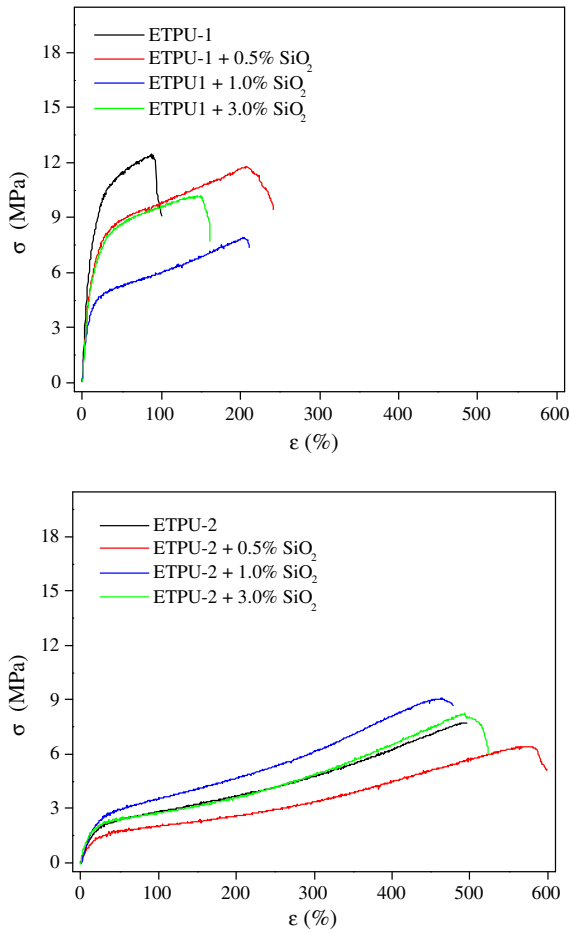

Fig. 12. Stress–strain curves of silica nanocomposite films of ETPU-1 and ETPU-2 at different strain levels.

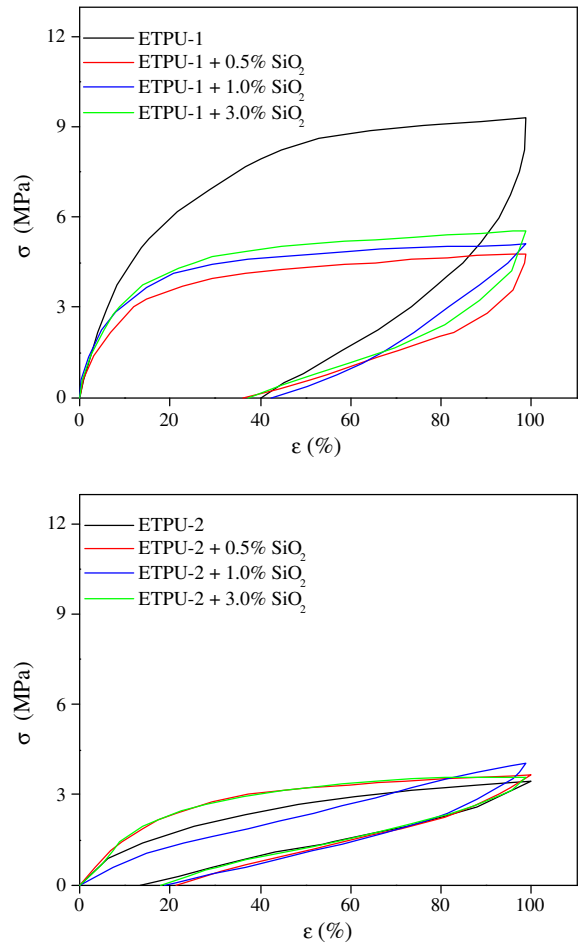

Fig. 13. The cyclic stress–strain behavior of ETPU-1 and ETPU-2 nanocomposite films loaded to 100% strain.

Table 3
Tensile behavior of ETPU matrices and nanocomposites.

Composite	Young modulus E (MPa)	Stress at break [a] σ (MPa)	Strain at break [b] ε_b (%)	Work to break W (Nm)
ETPU-1 HSC = 51%	107.8	12.5	100.2	0.14
ETPU-1 + 0.5% SiO_2	90.4	11.9	249.9	0.49
ETPU-1 + 1.0% SiO_2	70.5	7.9	209.0	0.31
ETPU-1 + 3.0% SiO_2	48.6	10.2	161.1	0.24
ETPU-2 HSC = 34%	15.1	7.8	496.5	0.78
ETPU-2 + 0.5% SiO_2	13.0	6.5	599.2	0.63
ETPU-2 + 1.0% SiO_2	18.0	9.1	477.8	0.86
ETPU-2 + 3.0% SiO_2	33.9	8.3	524.0	0.70

[a] Stress at break or tensile strength.
[b] ε_b, elongation at break.

Table 4
Hysteresis behavior of ETPU matrices and nanocomposites – 50% strain.

Composite	W[a]	Permanent set[b]
ETPU-1 HSC = 51%	392.24	3.40
ETPU-1 + 0.5% SiO_2	185.53	3.65
ETPU-1 + 1.0% SiO_2	258.23	3.90
ETPU-1 + 3.0% SiO_2	224.28	3.73
ETPU-2 HSC = 34%	54.73	2.80
ETPU-2 + 0.5% SiO_2	74.08	4.40
ETPU-2 + 1.0% SiO_2	68.05	2.90
ETPU-2 + 3.0% SiO_2	86.21	3.10

[a] Work done on the sample, in mJ.
[b] Displacement at relief (in mm) – the strain at zero stress in the unloading cycle [21].

maxima of the elongation at break plots at 0.05 wt.% of silica lack definiteness it is tempting to assume the same type of behaviour as the one demonstrated by Lee et al. [19]. In their case the maximum was found at around 2 wt.% with almost order of magnitude greater elongation at break. However, in our case the tensile plots do not show such a behavior. This may well be due to much larger aggregates of the silica nanoparticles in the polyurethane matrix present in our samples as a consequence of preparing ETPU without the nanosilica, i.e. they all were blended with the nanosilica.

The pure and nanocomposite samples were also subjected to mechanical hysteresis testing. A summary of the strain–hysteresis data obtained for uniaxially deformed

Table 5
Hysteresis behavior of ETPU matrices and nanocomposites – 100% strain.

Composite	W^a	Permanent set[b]
ETPU-1 HSC = 51%	484.72	9.35
ETPU-1 + 0.5% SiO_2	301.55	8.42
ETPU-1 + 1.0% SiO_2	309.60	9.44
ETPU-1 + 3.0% SiO_2	297.55	9.35
ETPU-2 HSC = 34%	111.59	5.20
ETPU-2 + 0.5% SiO_2	132.05	7.10
ETPU-2 + 1.0% SiO_2	89.14	7.20
ETPU-2 + 3.0% SiO_2	132.26	6.40

[a] Work done on the sample, in mJ.
[b] Displacement at relief (in mm) – the strain at zero stress in the unloading cycle [21].

films in a cyclic mode up to 50% and 100% strain is provided in Tables 4 and 5 (the data are for the specific samples used in the experiment and only the relative values matter). The mechanical hysteresis behavior of two series of ETPU nanocomposites loaded to 100% strain is presented in Fig. 13. Obviously, higher the HSC, greater the associated hysteresis is, especially at strains of 100%. According to the reported literature data [32], high level of hysteresis in polymers with high HSC, is due to the irreversible breaking of physical cross-links while low hysteresis is typically found in PU with hard domains isolated in an amorphous soft segment matrix. In any case, it seems that neither ETPU-1 nor ETPU-2 has high enough HSC for appreciable hysteresis to occur. Disruption of hydrogen bonding may not be an important cause of the mechanical hysteresis because stretching appears to have no effect on the hydrogen bond network. The set of urethane domains provide a molecular basis for the observed mechanical hysteresis [33].

3.4. Thermal properties

The DSC results obtained from the second run by scanning from −90° to 250° and the related thermal property data are summarized in Table 6 and shown in Fig. 14. Three transitions were observed in ETPU-1 and two in ETPU-2 samples. Transition around −44° corresponds to the glass transition (T_g) of soft segments. Transition at higher temperature around 100–240° corresponds to the melting

Table 6
Results of the DSC analysis of ETPU matrices and nanocomposites.

Composite	T_g [a]	T_m [b]	ΔT_m	ΔH_m [c]
ETPU-1 HSC = 51%	−44.7	187.9, 212.1	24.2	21.87
ETPU-1 + 0.5% SiO_2	−52.3	190.4, 208.0	17.6	21.44
ETPU-1 + 1.0% SiO_2	−47.9	186.6, 211.9	25.3	26.90
ETPU-1 + 3.0% SiO_2	−45.9	185.7, 209.1	23.4	25.78
ETPU-2 HSC = 34%	−45.9	112.5		3.17
ETPU-2 + 0.5% SiO_2	−47.5	109.9		5.42
ETPU-2 + 1.0% SiO_2	−46.2	106.0		4.66
ETPU-2 + 3.0% SiO_2	−43.2	100.9		5.29

[a] Glass transition temperature (in °) of soft segments.
[b] Crystal melting temperature.
[c] Heat of fusion (in J/g) of multiple peaks in ETPU-1 and of a single peak in ETPU-2.

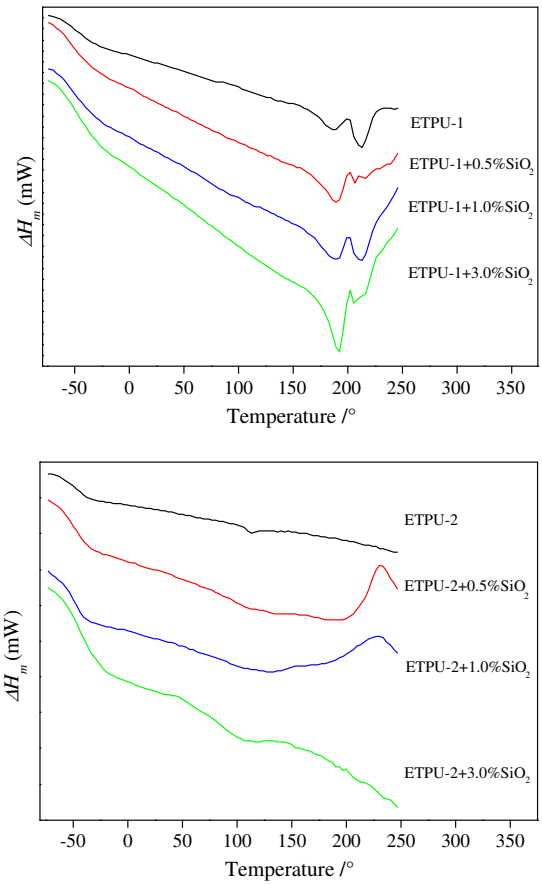

Fig. 14. DSC curves of ETPU-1 and ETPU-2 nanocomposite films.

(T_m) of hard segments crystallites [32]. Interestingly enough, the samples of Lee et al. [19] went trough the glass transition at about the same temperature but showed the melting transition due to the PTMEG (soft) segments at 25° and very broad and barely observable peak somewhere between 100° and 200° (not discussed in [19]). This contradicts the observation of Lee et al. [35] that the absence of the hard segment melting point is related to not using chain extenders in PU preparation. The absence of the soft segment melting point is related to the presence of aromatic hard segments, for example, MDI. The miscibility of soft and hard segments is in that case enlarged and this is accompanied with the absence of soft segment melting.

A large difference between the glass transition temperatures of soft and hard segments is a source of elastomeric properties. The elastomeric performance declines with the growing content of the hard segments. Therefore, the glass transition temperature (T_g) often is used as a measure of phase separation because it is primarily affected by the amount of hard segments dispersed in the soft segment phase. Actually, the broadness of the glass transition range depends on the amount of hard segments and their separation from the soft segments. It depends on the mobility of polymer chains, the more immobile the chains, the higher the value of T_g. In ETPU-1 the T_g was at −44.7° while for ETPU-2 with lower HSC (34% vs. 51%) the T_g was only

1.2° lower. Obviously the widths of the corresponding peaks have to be compared. Comparing the T_g values of the two nanocomposite series, the values obtained exhibit in either cases minima at 0.05 wt.% silica with the temperature difference of 5°. Similar observations were reported in segmented PU having SSC of 50 and 70 wt.% [34]. The soft segment T_g increases slightly with increasing hard segment content as a consequence the decreased mobility of the soft segments. The variation of soft segment T_g within only few degrees can be connected with the effect of hard segments on the mobility of soft segments.

The changes in the T_g of a polymer matrix induced by the addition of nanosized particles can take place in both directions [2] depending on the method of mixing and the size of nanoparticles. The PU silica nanocomposites obtained from *in situ* polymerization have much higher T_g than the corresponding nanocomposites prepared by blending method [36]. There are also examples of marginal changes of the T_g. In polyester PU the addition of SiO_2 nanoparticles with diameters in range (175–730) nm did not affect T_g of pristine polymer [37]. It was found that maximum values of T_g were obtained when the particle size of silica was about 28 nm [38]. With the addition of nanosilica in ETPU-1 and ETPU-2 samples, the T_g are first slightly shifted to lower temperatures as compared with neat samples. However, the shifting is small and obviously higher silica concentrations are needed to achieve more significant values.

The thermal properties are connected with mechanical and orientational behavior of ETPU nanocomposites. Because the Young's modules of the ETPU-1 composites decreased with increasing SiO_2 nanoparticles content, the glass transition temperature, as expected, also decreased (Tables 3 and 6) [39]. Since T_g is inversely proportional to the soft segments mobility, ETPU-1 nanocomposites exhibit enhanced mobility and thus decreased orientation of segments. The lowest values of orientational function and lowest T_g are obtained in ETPU-1 + 0.5% SiO_2 sample with highest elongation of break (Figs. 10 and 11.). This property can be explained by formation of an interfacial polymer layer (shell) attached to the particle core. In the case of repulsive forces between the particle and the interfacial layer, the polymer chain mobility is increased yielding in a plasticizing effect accompanied with decreased T_g [40,41] .

In ETPU-2 + 0.5% SiO_2 T_g and E were slightly lower in comparison to neat ETPU-2, the values of orientational function are not changed significantly. Further increase in SiO_2 content to 1% and 3% lead to increased T_g and E, the reduced mobility of chains is accompanied with enhanced orientation (Figs. 10 and 11.).

Melting of ETPU samples was also studied by DSC to indicate the degree of organizational order of crystalline domains through the melting behavior of the crystalline phase and the degree of interactions between nanofiller and hard and soft segments [34,42,43]. DSC measurements give in ETPU-1 samples two melting peaks (T_m) at around 190° and 210°. The multiple endothermic behaviour could be connected with the long-range order of the hard segments crystallites [42,43]. Some of the multiple melting peaks could be attributed to the hydrogen bond dissociation, for example, hard–hard segment or hard–soft segment hydrogen bonds as well as to various levels of packing order in the hard domains [44]. According to DSC results there is no significant effect of the nanofiller on the melting points on ETPU-1 samples. In all ETPU-2 samples only one endothermic peak was observed (Table 6). The melting point is decreased by ~12° with increasing nanosilica content. A single melting peak could be attributed to the disruption of short-range order within the hard segment microdomains [45]. The T_m is shifted toward a lower temperature for ETPU-2 nanocomposite which may be attributed to smaller crystallites of the hard segments [34].

4. Conclusions

The comprehensive IR linear dichroism study showed that in the case when the particles of the nanofiller can form hydrogen bonds with polymer segments it is necessary to analyze changes due to hydrogen bonding in several vibrations bands. The number of hydrogen bonded NH groups in either ETPU-1 or -2 remained almost constant after the incorporation of SiO_2 nanoparticles. DPS calculated from NH and C=O stretching vibrational bands was not affected significantly by addition of nanosilica. The number of hydrogen bonded carbonyl groups increased by 10% due to interactions with SiOH groups but only in the ETPU-1 samples. The addition of nanosilica into the ETPU-2 matrix showed no significant influence on the number of hydrogen bonded NH and C=O groups. The analysis of C–O stretching band in ether C–O–C groups has shown that in ETPU-1 nanocomposites SiO_2 particles interact only with hard segments. In ETPU-2 nanocomposites with 0.5% SiO_2 nanoparticles interact through hydrogen bonding with soft segments. Higher content of nanofiler reduced the number of bonded ether C–O–C groups in ETPU-2 nanocomposites influencing thus the interactions between hard and soft segments.

The addition of nano-SiO_2 particles into the ETPU-1 matrix with higher HSC decreases stiffness and strength but significantly increases elongation at break and toughness. Those features were attributed to the plasticizing effect due to the repulsive forces between interfacial layer and SiO_2 nanoparticles.

The behavior of ETPU-2 nanocomposite films with lower HSC was quite different. As SiO_2 loading increased, stiffness, tensile and toughness passes through a minimum at a particle concentration of 0.5 vol.% accompanied with maximal elongation at break. Compared to neat ETPU-2, nanocomposites with 1% and 3% SiO_2 showed slight reinforcement. The nanoparticles most probably act as hard segments thus increasing the Young's modulus.

The addition of nanofiller had small influence on the glass transition temperature T_g of the soft segments. The small changes in T_g are connected with mobility of segments influencing thus values of orientational function.

Melting behavior of ETPU was primarily affected by the hard segments. In ETPU-2 the introduction of nanofiller significantly decrease the crystal melting temperature which is accompanied with the increase in the melting endotherm enthalpy. There is an optimal silica content value which is around 1 vol.% giving an extreme value of tensile. By further increasing the content the tensile of the nanocomposite approaches to that of the neat substance.

The analysis had shown that results of spectroscopic investigation are correlated with the observed mechanical and thermal properties of ETPU nanocomposites.

Acknowledgment

The authors are grateful to Prof. Dr. Z. Veksli for fruitful discussions. This work was supported by the Ministry of Science and Technology of the Republic of Croatia (Projects 0982904-2927, 1252971-2868, 1252971-2575 and 1252971-2578).

References

[1] Mai YW, Yu ZZ, editors. Polymer nanocomposites. Cambridge, UK: Woodhead Publishing Limited Cambridge; 2006.
[2] Paul DR, Robeson LM. Polymer nanotechnology: nanocomposites. Polymer 2008;49(15):3187–204.
[3] Kickelbick G. Concepts for the incorporation of inorganic building blocks into organic polymers on a nanoscale. Prog Polym Sci 2003;28(1):83–114.
[4] Bistričić L, Leskovac M, Baranović G, Lučić Blagojević S. Mechanical properties and linear infrared dichroism of thin films of polyurethane nanocomposites. J Appl Polym Sci 2008;108(2):791–803.
[5] Barus S, Zanetti M, Lazzari M, Costa L. Preparation of polymeric hybrid nanocomposites based on PE and nanosilica. Polymer 2009;50(12):2595–600.
[6] Chen C, Justice RS, Schaefer DW, Baur JW. Highly dispersed nanosilica–epoxy resins with enhanced mechanical properties. Polymer 2008;49(17):3805–15.
[7] Bokobza L, Chauvin JP. Reinforcement of natural rubber: use of in situ generated silicas and nanofibres of sepiolite. Polymer 2005;46(12):4144–51.
[8] Krol P. Synthesis methods, chemical structures and phase structures of linear polyurethanes. Properties and applications of linear polyurethanes in polyurethane elastomers, copolymers and ionomers. Prog Mater Sci 2007;52(6):915–1015.
[9] Ji FL, Hu JL, Li TC, Wong YW. Morphology and shape memory effect of segmented polyurethanes. Part I: with crystalline reversible phase. Polymer 2007;48(17):5133–45.
[10] Gunes IS, Cao F, Jana SC. Evaluation of nanoparticulate fillers for development of shape memory polyurethane nanocomposites. Polymer 2008;49(9):2223–34.
[11] Yilgor I, Yilgor E, Guclu Guler I, Wars TC, Wilkes GL. FTIR investigation of the influence of diisocyanate symmetry on the morphology development in model segmented polyurethanes. Polymer 2006;47(17):4105–14.
[12] Vega-Baudrit J, Navarro-Banon V, Vasquez P, Martin-Martinez JM. Addition of nanosilicas with different silanol content to thermoplastic polyurethane adhesives. Int J Adhes Adhes 2006; 26(5):378–87.
[13] Vega-Baudrit J, Sibaja-Ballestero M, Vazquez P, Torregrsa-Macia R, Martin-Martinez JM. Properties of thermoplastic polyurethane adhesives containing nanosilicas with different specific surface area and silanol content. Int J Adhes Adhes 2007;27(6):469–79.
[14] Petrović ZS, Javni I, Waddon A, Banhegyi G. Structure and properties of polyurethane–silica nanocomposites. J Appl Polym Sci 2000; 76(2):133–51.
[15] Nunes RCR, Fonseca JLC, Pereira MR. Polymer–filler interactions and mechanical properties of a polyurethane elastomer. Polym Test 2000;9(1):93–103.
[16] Nunes RCR, Pereira RA, Fonseca JLC, Pereira MR. X-ray studies on compositions of polyurethane and silica. Polym Test 2001;20(6): 707–12.
[17] Zhou S-X, Wu L-M, Sun J, Shen W-D. Effect of nanosilica on the properties of polyester-based polyurethane. J Appl Polym Sci 2003;88(1):189–93.
[18] Meckel W, Goyert W, Wieder W. Thermoplastic polyurethane elastomers. In: Legge NR, Holden G, Schroeder HE, editors. Thermoplastic elastomers. Munich: Hauser Publishers; 1987. p. 13–46.
[19] Lee S-I, Hahn YB, Nahm KS, Lee Y-S. Synthesis of polyether-based polyurethane–silica nanocomposites with high elongation property. Polym Adv Technol 2005;16(4):328–31.
[20] Saunders JH, Frisch KC. Polyurethanes chemistry and technology, part I. New York: Interscience Publisher; 1962. p. 32–44.
[21] Xu Y, Petrovic Z, Das S, Wilkes GL. Morphology and properties of thermoplastic polyurethanes with dangling chains in ricinoleate-based soft segments. Polymer 2008;49(19):4248–58.
[22] Tien YI, Wei KH. Hydrogen bonding and mechanical properties in segmented montmorillonite/polyurethane nanocomposites of different hard segment ratios. Polymer 2001;42(7):3213–21.
[23] Sun H. Ab initio characterizations of molecular structures, conformation energies, and hydrogen-bonding properties for polyurethane hard segments. Macromolecules 1993;26(22): 5924–36.
[24] Bandekar J, Klima S. FT-IR spectroscopic studies of polyurethanes Part II. *Ab initio* quantum chemical studies of the relative strengths of "carbonyl" and "ether" hydrogen-bonds in polyurethanes. Spectrochim Acta 1992;48A(10):1363–70.
[25] Bandekar J, Klima S. FT-IR spectroscopic studies of polyurethanes. Part I. Bonding between urethane C–O–C groups and the NH Groups. J Mol Struct 1991;263:45–57.
[26] Seymour RW, Estes GM, Cooper SL. Infrared studies of segmented polyurethan elastomers. I. Hydrogen bonding. Macromolecules 1970;3(5):579–83.
[27] Yilgör E, Yilgör I, Yurtsever E. Hydrogen bonding and polyurethane morphology. I. Quantum mechanical calculations of hydrogen bond energies and vibrational spectroscopy of model compounds. Polymer 2002;43(24):6551–9.
[28] Ikeda R, Chase B, Everall NJ. Basic of orientation measurements in infrared and Raman spectroscopy. In: Everal NJ, Chalmers JM, Griffiths PR, editors. Vibrational spectroscopy of polymers: principles and practice. Wiley; 2007. p. 306.
[29] Gede UW, Wiberg G. Development and relaxation of orientation in pure polymer liquid crystals and blends. In: Brostow W, editor. Mechanical and thermophysical properties of polymer liquid crystals and blends. London: Chapman and Hall; 1998. p. 283.
[30] Lee H-S, Ko J-H, Song K-S, Choi K-H. Segmental and chain orientational behavior of spandex fibers. J Polym Sci Part B Polym Phys 1997;35(11):1821–32.
[31] Merabia S, Sotta P, Long DR. A microscopic model for the reinforcement and the nonlinear behavior of filled elastomers and thermoplastic elastomers (Payne and Mullins effects). Macromolecules 2008;41(21):8252–66.
[32] Gorce JN, Hellgeth JW, Ward TC. Mechanical hysteresis of a polyether polyurethane thermoplastic elastomer. Polym Eng Sci 1993;33(18):1170–6.
[33] Estes GM, Seymour RW, Cooper SL. Infrared studies of segmented polyurethane elastomers. II. Infrared dichroism. Macromolecules 1971;4(4):452–7.
[34] Petrović ZS, Cho YJ, Javni I, Magonov S, Yerina N, Schaefer DW, et al. Effect of silica nanoparticles on morphology of segmented polyurethanes. Polymer 2004;45(12):4285–95.
[35] Lee D-K, Tsai H-B. Properties of segmented polyurethanes derived from different diisocyanates. J Appl Polym Sci 2000;75(1):167–74.
[36] Chen Y, Zhou S, Yang H, Gu G, Wu L. Preparation and characterization of nanocomposite polyurethane. J Colloid Interface Sci 2004;279(2):370–8.
[37] Gonzalez-Irun-Rodriguez J, Carreira P, Garcia-Diez A, Hui D, Artiaga R, Liz-Marzan LM. Nanofiller effect on the glass transition of a polyurethane. J Therm Anal Calorim 2007;87(1):45–7.
[38] Chen Y, Zhou S, Yang H, Wu L. Structure and properties of polyurethane/nanosilica composites. J Appl Polym Sci 2005;95(5): 1032–9.
[39] Perez LD, Giraldo LF, Brostow W, Lopez BL. Poly(methyl acrylate) plus mesoporous silica nanohybrids: mechanical and thermophysical properties. e-Polymers 2007;29:1–11.
[40] Hanneman T, Vinga Szabo D. Polymer–nanoparticle composites: from synthesis to modern applications. Materials 2010;3:3468–517.
[41] Li G, Kancheng M, Feng K. Plasticization of nano-$CaCO_3$ in polystyrene/nano-$CaCO_3$ composites. J Appl Polym Sci 2006;99: 2138–43.
[42] Leung LM, Koberstein JT. DSC annealing study of microphase separation and multiple endothermic behavior in polyether-based polyurethane block copolymers. Macromolecules 1986;19(3): 706–13.
[43] Koberstein JT, Russell TP. Simultaneous SAXS-DSC study of multiple endothermic behavior in polyether-based polyurethane block copolymers. Macromolecules 1986;19(3):714–20.
[44] Seymour RW, Cooper SL. DSC studies of polyurethane block polymers. J Polym Sci Part B Polym Lett 1971;9:689–94.
[45] Koberstein JT, Galambos AF. Multiple melting in segmented polyurethane block copolymers. Macromolecules 1992;25(21): 5618–24.